AIAA JOURNAL
Vol. 33, No. 3, March 1995

Structure of Supersonic Turbulent Boundary Layer After Expansion Regions

S. A. Arnette,* M. Samimy,† and G. S. Elliott‡
Ohio State University, Columbus, Ohio 43210

The effects of four expansion regions [centered and gradual ($R/\delta_0 \simeq 50$) expansions of both 7 and 14 deg] on a fully developed Mach 3 turbulent boundary layer were investigated. Instantaneous visualizations were made possible by the presence of scalar water condensation in the freestream and its absence in the higher temperature boundary layer. The elongated longitudinal structures previously found in the flat plate boundary layer are present downstream of the expansions. Large-scale structures increase in scale across the expansions. Structure angles also initially increase but are found to return to the flat plate value $10\delta_0$ downstream of the 7-deg centered expansion. The rapid quenching of small-scale turbulence by the expansions results in a more intermittent boundary layer visually dominated by large-scale structures. Convection velocities derived from double-pulse correlations are reasonable in the flat plate and 7-deg centered expansion boundary layers. Excess condensation downstream of the 14-deg expansions (probably CO_2) made the 14-deg expansion results more difficult to interpret.

Nomenclature

n	= normal distance above the surface
R	= radius of curvature for the gradual expansions, correlation coefficient
Re_θ	= Reynolds number based on boundary layer momentum thickness
s	= streamwise distance along the surface measured from the start of the convex curvature
$\boldsymbol{U}$	= mean velocity vector
U	= mean streamwise velocity
u_τ	= friction velocity
V	= mean normal velocity
x	= horizontal distance measured from $(s, n) = (0, 0)$
y	= vertical distance measured from $(s, n) = (0, 0)$
Δp	= pressure difference across the expansion region
δ_0	= boundary layer thickness at $s = 0$ mm
δ_{vis}	= boundary layer thickness defined by 99% of the freestream intensity
δ_{RMS}	= normal distance above the boundary where the peak in the rms profile occurs
θ	= boundary layer momentum thickness
ν	= kinematic viscosity
τ_0	= surface shear stress ahead of the expansion region

Introduction

IMPROVED understanding of compressible turbulent boundary layers will always offer the potential for significant advances in high-speed flight applications as boundary layers are of such central importance to issues of drag and heat transfer. Although an increasingly detailed characterization of two-dimensional, flat plate, zero pressure gradient, compressible turbulent boundary layers continues to emerge,[1] it is rare that such canonical flows occur in applications. Instead, the boundary layer likely experiences several extra rates of strain caused by effects such as pressure gradients and streamline curvature.[2] Boundary-layer response to such perturbations is nonlinear, so that the effect of multiple perturbations cannot be predicted even if their individual effects are known.[3] Thus, studies of boundary layers subjected to multiple perturbations are needed.

Although our understanding of the effects of mean compression or dilatation on supersonic turbulent boundary layers is not very advanced, such effects are intuitively connected to the principle of conservation of angular momentum in the presence of the distortion of a mass element.[2] The passage of a two-dimensional, compressible turbulent boundary layer through an expansion is depicted in Fig. 1. In the expansion, the boundary layer encounters stabilizing convex streamline curvature, a favorable streamwise pressure gradient ($\partial p/\partial s < 0$), a normal pressure gradient ($\partial p/\partial n > 0$), and bulk dilatation ($\nabla \cdot \boldsymbol{U} > 0$). The mean velocity divergence within the expansion region ($\partial U/\partial x > 0$, $\partial V/\partial y > 0$ in the coordinate system of Fig. 1) and streamline curvature ($\partial V/\partial x < 0$) cause fluid elements' cross-sectional area to increase in the x–y, x–z, and y–z planes. As a result, all vorticity components are damped, resulting in an overall stabilization. References 4–12 are most of the relevant studies known to the authors. As discussed by Spina et al.,[1] past work illustrates the effects of dilatation over those of streamline curvature, i.e., $\nabla \cdot \boldsymbol{U} \gg \partial V/\partial x$ (a disparity that is enhanced with increasing Mach number).

Thomann[5] isolated the effects of 20 deg of gradual convex curvature on the heat transfer beneath a supersonic, turbulent boundary layer ($M_\infty = 2.5$) by eliminating pressure gradients with an appropriately shaped body in the freestream. The heat transfer rate decreased by approximately 20%, suggesting a significant reduction in turbulent mixing.

Dussauge and Gaviglio[6] investigated the 12-deg centered expansion of an $M_\infty = 1.76$ boundary layer ($\delta_0 = 10$ mm, $Re_\theta = 5\times10^3$). In addition to mean and turbulence measurements, an analysis based on Rapid Distortion Theory isolated the effect of bulk dilatation. Mean velocity profiles downstream of the expansion region initially displayed a thick sublayer region possessing a larger streamwise velocity gradient than that found in the incoming profile, with no apparent logarithmic region. After approximately $9\delta_0$, a logarithmic region reappeared. The calculations indicated the decreases in streamwise turbulence intensity sustained through the expansion were due primarily to bulk dilatation, although the reductions near the wall were not reproduced well by the calculations including only dilatation effects. After the expansion, the turbulence intensity near the wall ($n/\delta < 0.2$) was initially very low relative to incoming levels. For $n/\delta > 0.25$, the drop in turbulence intensity decreased with increasing normal distance. The near-wall region established turbulence intensities comparable to incoming levels more quickly than the outer portions of the boundary layer, where the evolution was slow. This is a consequence of the turbulence production being confined to the near-wall region that possesses significant mean

Received May 13, 1994; revision received Nov. 1, 1994; accepted for publication Nov. 28, 1994.

*Graduate Student, National Science Foundation Fellow, Department of Mechanical Engineering. Student Member AIAA.

†Professor, Department of Mechanical Engineering. Associate Fellow AIAA.

‡Postdoctoral Researcher, Department of Mechanical Engineering. Member AIAA.

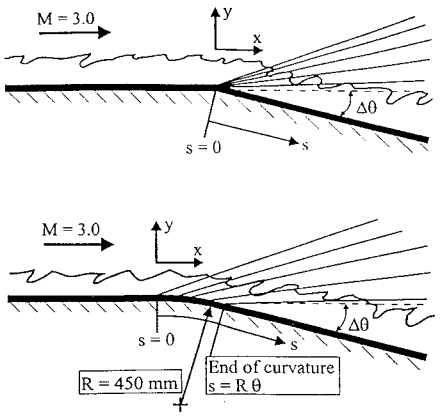

Fig. 1 Schematics of the a) centered and b) gradual expansion models ($\Delta\theta$ = 7 and 14 deg for both). The (x, y) origin is at the curvature onset at the surface. The n coordinate is zero at the surface and everywhere normal to the surface.

gradients. The rapid recovery of the near-wall region led to the proposal that a new internal layer had been formed after the expansion and that the boundary layer had been relaminarized.

A relaminarized boundary layer is defined as one in which the effects of the Reynolds stresses on the mean flow have become negligible.[13] It can occur when a turbulent boundary layer is subjected to a large, favorable pressure gradient. For expanded compressible turbulent boundary layers, Narasimha and Viswanath[12] suggest that relaminarization occurs for $\Delta p/\tau_0$ greater than approximately 70.

Smith and Smits[7] investigated the 20-deg centered expansion of an $M_\infty = 2.84$ ($\delta_0 = 26$ mm, $Re_\theta = 7.76 \times 10^4$) turbulent boundary. Mean and turbulence profiles were measured $1\delta_0$ upstream and $3.5\delta_0$ downstream of the corner. Again, the mean velocity profile did not possess a logarithmic region at $s/\delta_0 = 3.5$. The streamwise turbulence intensity and normal Reynolds stress were significantly decreased across the expansion, but the streamwise mass-flux fluctuation profile was essentially unchanged, suggesting more significant density fluctuations after the expansion. Calculations similar to those of Ref. 6 again showed the decreases in turbulence levels across the expansion were due mainly to dilatation.

Dawson et al.[10] acquired multipoint measurements of the fluctuating surface pressures in the expanded supersonic turbulent boundary layers of this study. Normalized power spectral densities were much more concentrated at low frequencies just downstream of the expansions relative to upstream, with accompanying sharp decreases at high frequencies. This suggested small-scale motions are quenched almost immediately by the expansion regions. Streamwise space–time correlations in the flat plate boundary layer showed the convection velocity to be 0.80–0.90 U_∞, which agrees well with other studies.[14] However, convection velocities were unreasonably high downstream of the expansions. These results suggest the relationship between the pressure field and the large-scale structures is severely altered by the expansions, which might be related to the wave propagation of acoustic disturbances relative to the mean flow velocity.[10] Such an effect has been demonstrated in a spatially simulated, turbulent, supersonic flow.[15]

It has become increasingly clear that turbulent boundary layers contain nonrandom, coherent structure. Impetus for investigating these structures comes from the discovery that they are of major importance to the dynamics of the turbulence. Our knowledge of coherent structures in compressible boundary layers is limited to the δ-scale motions of the outer layer.[1,16] This is in sharp contrast to the incompressible case, where several structural features have been investigated.[16] The reason is a lack of both spatial and temporal resolution.[17] Discussions of coherent structure in supersonic turbulent boundary layers are given elsewhere.[1,9,11,14,17]

Plan view visualizations in the Mach 3 flat plate boundary layer of this study reveal structures of a very large streamwise, and limited spanwise, extent.[9,11,18] As such, these elongated longitudinal structures are somewhat similar to those near the wall of incompressible boundary layers. However, these structures were found well above the inner layer, nominally at $n/\delta = 0.5$–1.0, and have a larger spanwise extent than near-wall streaks of incompressible cases. Although the structures are possibly present deeper in the boundary layer, the visualization technique precluded visualizations closer to the wall. The removal of the flow conditioning assembly had little or no effect on the presence of the elongated structures. These facts suggest the structures may be a robust feature of the compressible boundary layer, although no comment could be made on their importance. Their apparent absence in incompressible boundary layers calls to question longstanding ideas concerning the similarity of the turbulence structure of incompressible and compressible boundary layers.[18]

This work is part of an ongoing study of the effects of expansion regions on supersonic turbulent boundary layers. A more complete presentation of the results appears elsewhere.[11]

Experimental Procedure

The experiments were performed at the Aeronautical and Astronautical Research Laboratory at the Ohio State University. The boundary layer develops on a flat plate from the stagnation chamber to the beginning of the convex surface curvature (67 cm from the throat to the beginning of the surface curvature). The incoming Mach 3 flow occupies a passage 152.4 mm wide by 76.2 mm high. After the expansion regions, the model surfaces diverge away from the expansion corner towards the bottom of the test section, which has a total cross section of 152.4 mm wide by 152.4 mm high. This configuration and the employed coordinate system is illustrated in Fig. 1. Optical access is provided by windows in the top and side walls. The system has a storage capacity of 42.5 m^3 at pressures up to 16.4 MPa. The stagnation pressure was 1.14 MPa (11.2 atm) $\pm 1\%$, and the stagnation temperature was nominally 280 K. The stagnation chamber is equipped with a removable flow conditioning section consisting of a perforated plate, a 10-cm honeycomb section, and a screen. Previous laser Doppler velocimetry (LDV) measurements by Samimy et al.[19] showed the freestream streamwise and normal turbulence intensities to be less than 3%. At the location corresponding to the start of the four expansion regions the results were $M_\infty = 3.01$, $\delta_0 = 9.2$ mm, $\theta = 0.37$ mm, and $Re_\theta = 2.47 \times 10^4$.

The centered and gradual expansion geometries are depicted in Fig. 1. The radius of curvature for both gradual expansion models is 450 mm, giving $R/\delta_0 \simeq 50$. In addition to the four expansion models, a flat plate model was used to extend the incoming boundary layer through the length of the test section. It includes a flush-mounted window (20 mm by 310 mm) along its centerline to reduce surface reflections.

Schlieren photography was used to ensure no freestream nonuniformities were present. Spanwise and streamwise distributions of mean static pressures at the model surfaces were monitored via static taps in the models. Schlieren images[9–11] and mean pressure measurements[9,10] are presented elsewhere.

Small particles of condensed water form in the nozzle during the expansion to Mach 3, creating a scalar marker in the freestream. The condensate comes from the small amount of water vapor left in the supply air after passing through the system's desiccant dryers, which reduce the compressed air's water content to very low levels. Condensate is not formed in the higher temperature boundary layer. This provides an approximate indicator for visually differentiating the turbulent boundary layer from the freestream. The high sensitivity of the collected signal to the incident polarization direction suggests the scattering falls near the Rayleigh regime, giving an effective particle diameter on the order of 50 nm for the employed 532-nm illumination. This suggests the particles are sufficiently small to accurately follow the marked fluid. Similar condensation visualizations of compressible turbulent boundary layers have been obtained with uv Rayleigh scattering.[20]

Most visualizations were acquired with the filtered Rayleigh scattering (FRS) technique, originally proposed by Miles et al.[21]

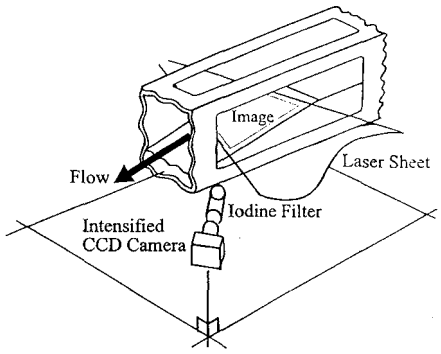

Fig. 2 Schematic of the laser sheet and camera/filter configuration for the global plan views.

FRS has been successfully applied in supersonic jets,[22] mixing layers,[23] and boundary layers[9,11,18] and has been discussed in detail elsewhere.[21,24–26] An optical cell containing diatomic iodine vapor is used as a frequency discriminator. Diatomic iodine possesses electronic transitions that absorb the frequency-doubled 532-nm radiation of the Nd:YAG laser.[21] The cumulative absorption of the iodine molecules forms a notch filter. The absorption profile can be modified by changing the thermodynamic state of the iodine vapor[21] or the gas composition.[26] Scattering from the condensed particles in the flow is positively Doppler shifted for appropriate optical configurations. Assuming the particles insensitive to molecular motions, the line width of the scattering is simply that of the interrogating laser. By using an injection-seeded Nd:YAG laser, the laser line width is narrow enough that, when the laser frequency is properly tuned, the filter will absorb background reflections (at the laser frequency) while passing Doppler shifted scattering from the condensate.

Several sheet orientations were employed for the FRS visualizations. For streamwise views the sheet entered the test section from the top, and for spanwise views it entered from the side. For both, the camera was rotated 45 deg downstream from the spanwise direction to obtain a positive frequency shift. For the acquisition of global plan views, obtaining a frequency shift that sufficiently separated the condensed particle scattering and the background reflections required that the camera/filter be rotated downstream approximately 45 deg from the spanwise-aligned axis of the laser sheet (which entered from the side). To view the laser sheet, the camera/filter was elevated. For the flat plate, the camera was elevated approximately 35 deg above the plane of the laser sheet. For the expansion models, this angle was increased by approximately the expansion angle, i.e., the sheet was kept parallel to the surface and the camera was placed in nominally the same position in the laboratory frame. This configuration is illustrated in Fig. 2. The pulse duration of the Nd:YAG laser is 9 ns, which effectively freezes the flow. The frequency-doubled Nd:YAG laser is capable of 660 mJ/pulse.

Double-pulse streamwise images of the flat plate and two centered expansion boundary layers were acquired with standard laser sheet lighting of the condensation. The Nd:YAG laser can provide two pulses for each lamp excitation by multiple Q-switching. The delay between the initial and delayed light pulses, which can be set between 15 and 200 μs, was measured with an oscilloscope. To reduce reflections at the boundaries, the centered expansion models were equipped with centered, flush-mounted windows approximately 20 mm wide.

Images were collected with Princeton Instruments 14-bit intensified charge-coupled device (CCD) cameras and stored on 486DX personal computers. Two of these systems were used in the double-pulse experiments. The framing rates (2–3 Hz) result in consecutive images being uncorrelated. The laser provides outputs for camera synchronization, one in single-pulse mode and two in double-pulse mode. The camera controllers possess circuitry such that each will wait until the other is ready to acquire an image (finished storing the previous image) before acquiring an image at the appropriate pulse of the laser's next double pulse. Double-pulsed Nd:YAG lasers have been used in other studies of compressible boundary layers[27,28] and mixing layers.[29]

Results and Discussion

The boundary-layer thickness increases across the expansions, which is expected given the sustained decrease in density. Schlieren images suggest the boundary-layer thickness increases by factors of approximately 1.5 and 2.0 for the 7- and 14-deg expansions, respectively.[10] A standard inviscid analysis gives pressure ratios (p_2/p_1) of 0.56 for the 7-deg expansions and 0.30 for the 14-deg expansions. The measured ratios were 0.53 (0.60) for the 7-deg centered (gradual) case and 0.36 (0.41) for the 14-deg centered (gradual) case.[10,11]

The method of Narasimha and Viswanath[12] was used to estimate the incoming skin friction coefficient in examining the criterion that relaminarization occurs for $\Delta p/\tau_0 > 75$. For the 7- and 14-deg centered expansions, this method gives $\Delta p/\tau_0$ estimates of 48 and 76, respectively. Since relaminarization is sensitive to the magnitude of the favorable pressure gradient, the 14-deg gradual expansion is not considered close to relaminarization. Despite satisfying the criterion, Smith and Smits[7] caution against the term relaminarization based on their cited mass flux fluctuation measurements in a Mach 3 boundary layer subjected to a 20-deg centered expansion. In the flows of this study, the ratio of rms surface fluctuation to local static surface pressure never drops below the flat plate value, which does not give an indication of relaminarization.[10]

Instantaneous streamwise FRS visualizations of the flat plate boundary layer are presented in Fig. 3. In the images, the flow is from right to left. In these and all other visualizations, added white lines indicate the position of the solid surface. The outer portions of the boundary layer are dominated by the presence of large-scale structures that display the presence of smaller scale motions at their outer edges. However, these smaller motions are too large to be identified with Falco's[30] typical eddies at the current Reynolds number ($Re_\theta \simeq 2.5 \times 10^4$). Motions of this scale in compressible boundary layers must be considered to scale on outer layer variables.[14] Similar to Smith and Smits,[31] instantaneous schlieren images of the boundary layer display downstream-inclined structures that span the entire boundary layer thickness.

Spanwise visualizations of the incoming boundary layer 25 mm upstream of the beginning of the expansion regions ($s = -25$ mm) are presented in Fig. 4. The large δ-scale structures of the outer layer are of limited spanwise extent, giving the top edge of the boundary layer a highly intermittent appearance.

Streamwise views of the boundary layer evolution through the 7-deg centered expansion are presented in Fig. 5. As in Figs. 5a and 5b, most large-scale structures increase in scale across the expansion. Recognizing a large-scale structure as a correlated mass of fluid, the sustained decrease in density would necessitate an increase in scale. Further, most structures just downstream of the expansion display a structure angle (relative to the downstream boundary) markedly

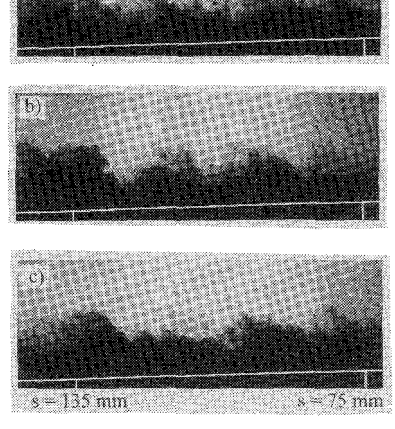

Fig. 3 Instantaneous FRS streamwise views of the flat plate boundary layer. The added white lines indicate the model surface. Indicated distances are relative to s = 0 mm (onset of expansion regions with expansion model installed).

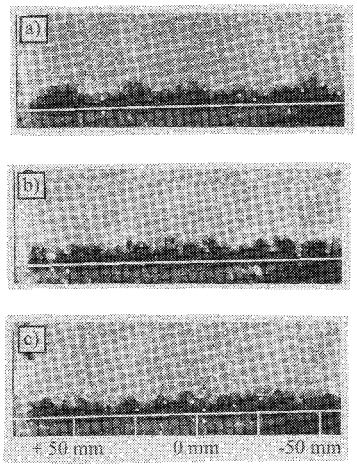

Fig. 4 Instantaneous FRS spanwise views of the flat plate boundary layer 25 mm upstream of the expansion regions. White lines indicate the model surface.

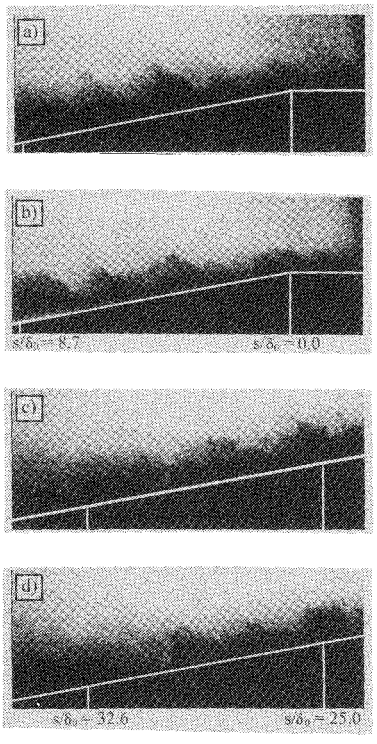

Fig. 5 Instantaneous FRS streamwise views downstream of the 7-deg centered expansion. Added white lines indicate the model surface.

greater than the flat plate value. A consideration of the kinematics of the passage of a large-scale structure through an expansion gives the probable explanation. Previous studies[14,17,32] have shown the large-scale structures are inclined to the wall at approximately 45 deg. The forward boundary of an expansion is inclined at 19.5 deg for a Mach 3 incoming flow. Although the forward boundary is inclined at larger angles closer to the surface because of the boundary-layer Mach number distribution, Mach angles close to 45 deg (which corresponds to $M = 1.41$) are confined very close to the surface. Thus the bottom of a structure will encounter the expansion region before the top. In addition, the diverging geometry of the expansion fan will cause the bottom of a structure to be accelerated through the expansion before the top. These two effects would result in an increased structure angle. Streamwise images acquired further downstream of the 7-deg centered expansion are presented in Figs. 5c and 5d. The boundary layer has a fuller appearance than it did just downstream of the expansion corner. Although large-scale structures corrugate the top edge of the boundary layer, the presence of smaller scales within the boundary layer makes their presence less obvious.

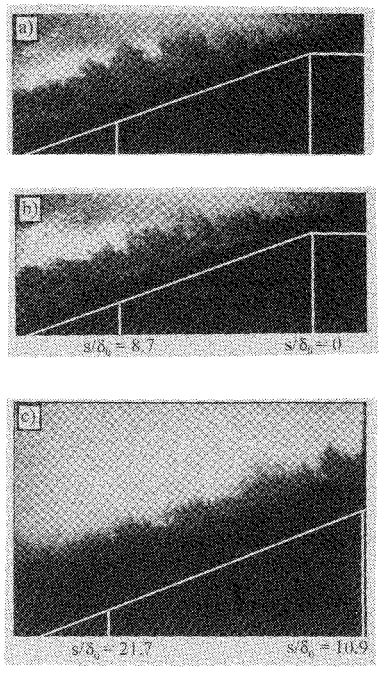

Fig. 6 Instantaneous FRS streamwise views downstream of the 14-deg centered expansion. Added white lines indicate the model surface.

Streamwise views of the 14-deg centered expansion region are presented in Figs. 6a and 6b. Again, the structures sustain an increase in both scale and angle through the expansion. Several structures downstream of the corner in Figs. 6a and 6b are essentially perpendicular to the surface. In general, the increases in scale and angle were more significant for the 14-deg centered or gradual expansion than for the corresponding 7-deg expansion, as would be expected if the explanations cited earlier were responsible. Near the downstream edge of the images, condensation more intense than that in the freestream is found just above the "no-condensation" layer. This new condensate is believed to be CO_2. The CO_2 in the tunnel air is well beyond saturation at the freestream conditions downstream of the 14-deg expansions.[34]

Since the excess condensation provided such a stronger signal than the condensed water particles, the relative amounts of CO_2 and H_2O in the flow were examined. The fact that the existing H_2O vapor does not condense in this facility with a Mach 2 nozzle installed was utilized. The condensation of H_2O vapor in supersonic expansions occurs as a rapid collapse from a supersaturated state. The data compiled by Wegener and Mack[33] suggest that for this tunnel operated at Mach 2, approximately 70 K of supercooling should be expected for very low water vapor content. The static temperature drops 77 K in the Mach 2 nozzle between the throat and exit. Therefore, if the H_2O vapor in the flow became saturated at the Mach 2 nozzle throat, condensation similar to that in the Mach 3 flow would be expected. Thus, an upper bound estimate for the H_2O content of the dried supply air can be obtained by assuming saturation at the Mach 2 nozzle throat. If this is done, an H_2O content of 2.9×10^{-5} kg H_2O/kg air is obtained. For the standard atmosphere there are 4.6×10^{-4} kg CO_2/kg air. This shows that CO_2, if condensed, could give signal levels much higher than the H_2O condensation. In fact, condensed H_2O particles may serve as CO_2 condensation sites.

The CO_2 condensation was not encountered downstream of the 7-deg expansions. Further downstream of the 14-deg centered expansion (Fig. 6c), the CO_2 condensation fills a progressively larger region above the boundary layer. The boundary layer has a very nonintermittent appearance with little evidence of large-scale structures. The boundary layer assumed this appearance whenever the CO_2 condensation was present. It is not clear if this is due to the CO_2 condensation or due to a sharp decrease in the boundary layer's ability to entrain fluid condensation containing.

Spanwise views downstream of the 7-deg centered expansion are presented in Fig. 7. At $s/\delta_0 = 4.2$ (Fig. 7a), the large-scale structures have increased in vertical scale relative to the flat plate case. Also,

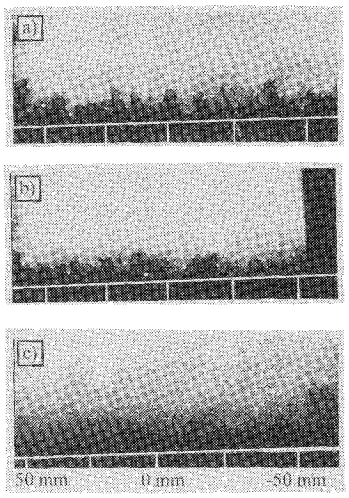

Fig. 7 Instantaneous FRS spanwise views of the boundary layer downstream of the 7-deg centered expansion at s/δ_0 of a) 4.2, b) 13.9, and c) 24.3 (δ_0 = 9.2 mm). Horizontal lines indicate the model surface.

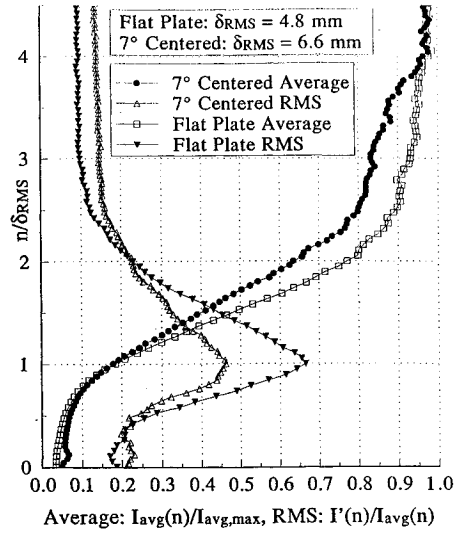

Fig. 8 Average intensity profile and rms intensity fluctuation profile for the flat plate and 7-deg centered expansion (s/δ_0 = 11.4) boundary layers.

the wells of fluid containing condensation penetrate deeper into the boundary layer than upstream of the expansion. Although the increase in vertical extent of the large-scale structures alone would cause these fluid wells to represent a larger fraction of the boundary-layer thickness, the quenching of smaller scale motions has given rise to more substantial penetrations. At $s/\delta_0 = 13.9$ (Fig. 7b) and 24.3 (Fig. 7c), the boundary layer is more full, suggesting a recovery of smaller scale motions. Spanwise views downstream of the other three expansions undergo the same progression. Results for the other expansions are given elsewhere.[11]

It seems that soon after the beginning of the expansion, small-scale motions are quenched. In fact, small-scale quenching was evident for the gradual expansion cases well before the end of the convex surface curvature. Qualitatively, the usual association of small scales with fluctuating vorticity seems appropriate. The conservation of angular momentum dictates that, given the encountered dilatation, small-scale fluctuating vorticity is damped (strictly true only in the absence of viscous effects). This, along with the usual association of small scales with the near-wall region, may help explain the sharp reductions in near-wall turbulence measured previously across centered expansions.[6,7] The survival of the larger scale motions through the expansions (which dominate the outer portions of the boundary layer) may explain the decreasing severity of reductions in turbulence intensity across expansions with increasing normal distance.[6,7]

Ensembles of streamwise views (200–250 images) were obtained of the flat plate (Fig. 3), 7-deg centered, and 14-deg centered expanded boundary layers. FRS was employed in the first two cases but was not needed for the latter case due to the CO_2 condensation. At the surveyed locations, the ensemble averages show the growth rate of the flat plate boundary layer is greater than that downstream of the 7-deg centered expansion, which in turn is greater than that downstream of the 14-deg centered expansion.[11]

Average intensity profiles and rms fluctuation profiles (normalized by the corresponding average profiles) for the flat plate and 7-deg centered expansion ($s/\delta_0 = 11.4$) boundary layers are presented in Fig. 8 (average profiles of 5 adjacent pixel columns). Normalizing with the elevation at peak rms (δ_{RMS}) is fairly effective in collapsing the average profiles. Further, δ_{RMS} represents a locally pertinent, obtainable parameter on which to base comparisons. It was chosen over δ_{vis} because of the difficulty encountered in accurately defining the elevation at which a certain percentage of the freestream intensity occurs. The average profiles suggest the boundary-layer thickness is approximately $3\delta_{RMS}$.

The rms profiles in Fig. 8 are reminiscent of rms temperature fluctuation profiles (normalized by local mean value) of supersonic turbulent boundary layers[34,35] in that a peak is present in the central portion of the boundary layer. This is very different from distributions of rms streamwise and normal velocity fluctuations, which monotonically decrease with increasing normal distance when normalized by local mean values.[34,35] Not surprisingly, this shows the condensation visualizations are most closely related to temperature. The mean temperature decreases from the surface to the top of the boundary layer, just the opposite of the average intensity. If the flat plate rms fluctuations are normalized by $[1 - I_{avg}(y)/I_{avg,max}]$, which is more representative of the mean temperature profile, the peak rms level is reduced by a factor of 4.3, giving a maximum of approximately 0.16 at $n/\delta_{vis} \simeq 0.3$. This compares fairly well to the maximum value of 0.08 found at $y/\delta \simeq 0.5$ in a Mach 3 boundary-layer temperature profile.[35] The remaining discrepancy may be partially due to the on-off nature of the condensation. Although mixed fluid at a given elevation in the boundary layer would be expected to occasionally possess the local mean temperature, fluid is either on or off in the visualizations depending on whether entrained condensation has been destroyed. The mean is determined mainly by the proportion of time condensation that is present and likely falls between the on and off extremes. Thus, higher rms levels are expected.

The rms peak downstream of the 7-deg centered expansion is only two-thirds of the flat plate rms peak (Fig. 8). The freestream rms, due mainly to fluctuations in laser intensity, is 0.10–0.15 for both cases, suggesting a direct comparison is valid. This reduction in peak rms is almost certainly related to the previously cited reduction of visual intermittency caused by the re-establishment of small-scale turbulence. If the outer layer were occupied only by large-scale structures, the fluid containing condensation upstream and downstream of the structures would give rise to large fluctuations about the mean, as in the flat plate boundary layer. However, the decreased growth rate downstream of the 7-deg centered expansion also suggests the large structures are weakened by the expansion, i.e., less able to entrain fluid, which might also be relevant to the reduced rms. Average and rms profiles for the boundary layer downstream of the 14-deg centered expansion were very different than those of Fig. 8 due to the CO_2 condensation and are presented elsewhere.[11]

Spatial correlations were calculated for the ensembles of instantaneous, streamwise visualizations. The correlations are unconditional in that a reference point is defined in the image space, the correlation field surrounding that point is calculated for each image, and the resulting correlation fields are then averaged over the ensemble. If an effective means of locating the reference point in a given image in a similar location relative to, or within, large-scale structures was derived, the average correlations would be a direct reflection of large-scale structure geometry and orientation. Since this is not done, a region of high correlation is not necessarily a result of large-scale structures (for example, if a reference point near the boundary-layer edge fell between the outer portions of adjacent large-scale structures). For this reason, the reference points were

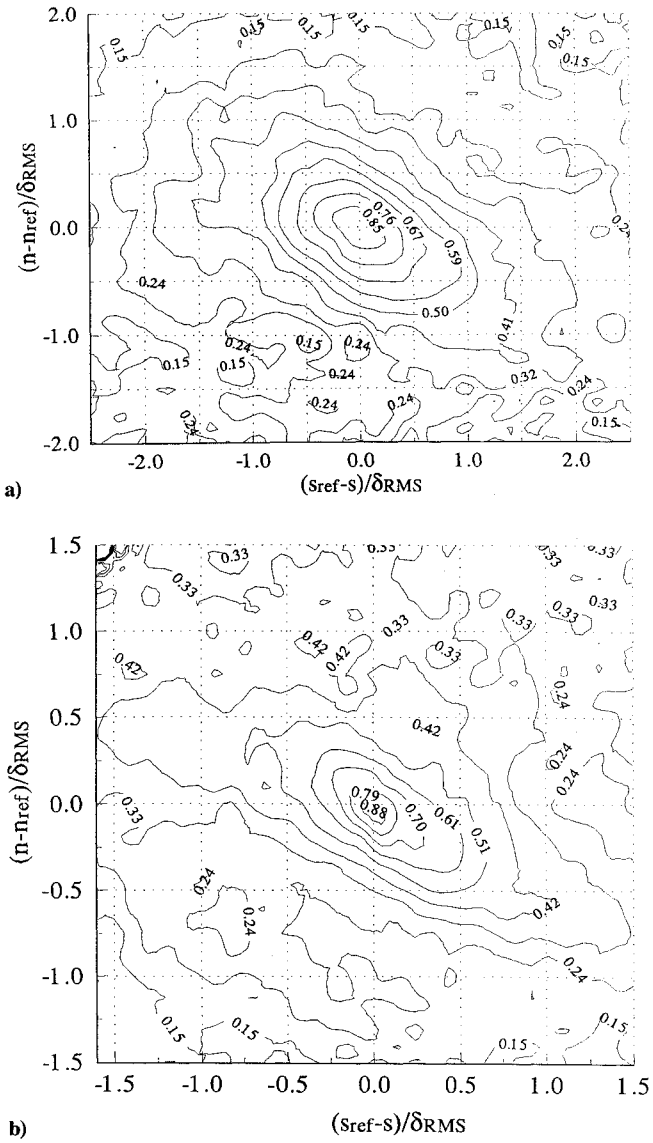

Fig. 9 Spatial correlations centered at n_{ref}/δ_{RMS} = 2.00 for a) the flat plate and b) the 7-deg centered expansion (s_{ref}/δ_0 = 9.2) boundary layers.

defined well within the boundary layer as defined by the average intensity profile. The employed formulas are presented elsewhere.[11,20] With this formulation, the correlation at the reference point is 1.00.

To draw relevant comparisons between the different cases, the normal length scale δ_{RMS} was used to locate the reference point. An ensemble correlation field for the flat plate boundary-layer streamwise views is presented in Fig. 9a. The reference point is located at $(s_{ref}, n_{ref}) = (13.0\delta_0, 2.0\delta_{RMS})$ where $\delta_0 = 9.2$ mm and $\delta_{RMS} = 4.2$ mm. For the spatial correlation fields, the streamwise direction is horizontal right to left. Normal and streamwise displacements have been normalized by δ_{RMS}. Thus, $(n-n_{ref})/\delta_{RMS} = -2.0$ corresponds to the surface. Recall, δ_{vis} is approximately equal to $3\delta_{RMS}$. Accordingly, this reference point is located well within the no-condensation region. As a result, correlations at higher elevations would be expected to occur only when large-scale structures are present. The contours slope downstream at approximately 45 deg, which is a result of the inclination of the large-scale structures. Similarly inclined contours were obtained by Smith et al.[20] Contours of significant correlation extend out to $n/\delta_{RMS} = 3.0$ and beyond, essentially to the top of the boundary layer as defined by the average intensity profile.

Ensemble spatial correlation fields obtained downstream of the 7-deg centered expansion, centered at $(s_{ref}, n_{ref}) = (9.2\delta_0, 2.0\delta_{RMS})$ where $\delta_{RMS} = 6.4$ mm, are presented in Fig. 9b. The correlation

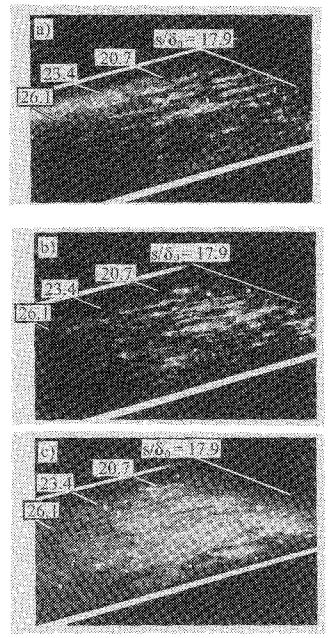

Fig. 10 Instantaneous FRS plan views of the boundary layer downstream of the 7-deg centered expansion (flow straighteners removed). The sheet is parallel to the surface at a) n = 4.5 mm, b) 6.5 mm, and c) 10.5 mm.

field is very similar to that of the flat plate case, with the regions of significant correlation having approximately the same dimensionless extent. Given the disparity in δ_{RMS} between the cases, the large scale structures are larger downstream of the expansion. Since δ_{RMS} is a similar fraction of δ_{vis} for the two cases, the increase in structure size nominally scales with the increase in δ_{vis} across the expansion. Similar to the flat plate case, the correlation contours are inclined at approximately 45 deg. Thus no increase in structure angle is apparent at this location. Although the structure angle appears larger just downstream of the expansion region (Fig. 5), it appears that the increase may not be long lasting. Spatial correlations downstream of the 14-deg centered expansion, given elsewhere,[11] bear no resemblance to those of Fig. 9. The dimensionless extent of significant correlation levels is significantly smaller than in Fig. 9, and the contours exhibit no downstream inclination. Again, this is probably related to the CO_2 condensation.

Figure 10 presents global plan views of the boundary layer at n = 4.5, 6.5, and 10.5 mm downstream of the 7-deg centered expansion. Recalling that the average intensity profile of Fig. 8 gives a δ_{vis} value of approximately 18 mm at $s/\delta_0 = 11.4$, these elevations are well within the boundary layer. The flow direction is from upper right to lower left. The spanwise extent of the test section is indicated by the lines aligned in the streamwise direction. Lines aligned in the spanwise direction have been added to give a sense of scale. The bright regions again indicate the presence of water condensation. Given the strong, negative correlation between temperature and streamwise velocity fluctuations in compressible turbulent boundary layers[1,6] and the fact that the condensation forms in the freestream, regions of condensation may be nominally considered high-speed fluid. Similar to plan views of the flat plate boundary layer,[9,11,18] the regions containing condensation appear as elongated structures nominally aligned in the streamwise direction. Because of the lack of condensation, it is not known if the elongated structures exist closer to the wall. The structures are less evident as the top of the boundary layer, and the more uniform condensation, is approached.

Removal of the flow conditioning elements (as was done for Fig. 10) has no noticeable effect on the elongated longitudinal structures in the plan views. That the elongated longitudinal structures survive the expansions and are present for such varied upstream conditions suggest they may be a robust feature of the compressible, turbulent boundary layer, although no comment can be made on their importance. The ensembles of plan views displaying the elongated longitudinal structures were averaged together to see if they

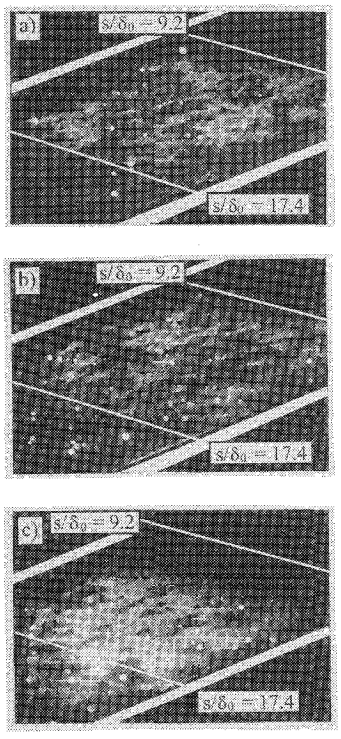

Fig. 11 Instantaneous FRS plan views of the boundary layer downstream of the 14-deg gradual expansion. The sheet is parallel to the surface at n = 10.0 mm (a and b) and n = 13.5 mm (c).

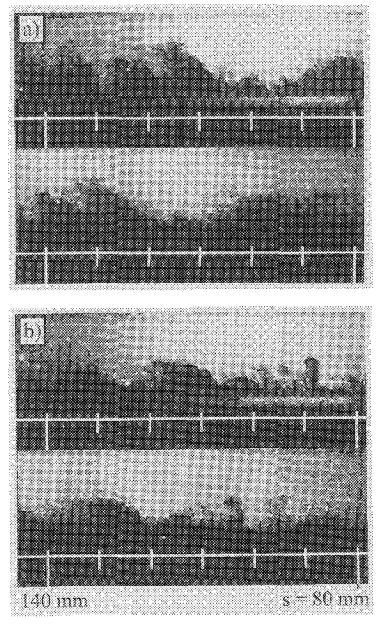

Fig. 12 Double-pulse streamwise views of the flat plate boundary layer. The bottom images were acquired 25.0 μs after the top images. The horizontal lines indicate the model surface.

occurred at specific spanwise locations, which might suggest a facility disturbance was responsible for the formation of the structures. However, all of the averaged images were uniform across the span. Results for all of the expansion cases are presented elsewhere.[11]

Figure 11 presents instantaneous plan views of the boundary layer downstream of the 14-deg gradual expansion at elevations of n = 10.0 mm (Figs. 11a and 11b) and 13.5 mm (Fig. 11c). The CO_2 condensation is present above the boundary layer, but the small amount of condensation present within the layer (probably H_2O) is imaged here. The appearance of the structures at greater normal elevations than in Fig. 10 is not surprising given the increase in boundary-layer thickness across the expansion. The elongated structures are clearly present at the lower elevation. Again, their presence is less clear with increasing normal distance.

Double-pulse visualizations of the flat plate boundary layer acquired with a time delay of 25.0 μs are presented in Fig. 12. The large-scale structures can be easily tracked from the initial to the delayed images. In many of the acquired image pairs the process of fluid entrainment is captured. As in Fig. 12, the entrainment process appears to typically consist of a forward rotation of the top of a large-scale structure. The rotation captures some fluid containing condensation and isolates it from the freestream. Such an occurrence would probably constitute a significant quadrant IV $\overline{uv}$ event. Entrainment into the boundary layer is indicated by the destruction of condensation originally present in the entrained fluid.

Quantitative information concerning large-scale structure convection can be gained from double-pulse images. Some have adopted the approach of identifying the centroids of large-scale structures, measuring the translation between the initial and delayed images, and calculating a velocity from the known time delay.[27,28] For the small time delays employed, the difficult task of identifying structure centroids gives rise to high uncertainties in structure velocities. Further, delineating rotation and convection is difficult. A second approach is to perform space–time correlations on ensembles of image pairs.[29] The presented correlations are based on 150 pairs of initial and delayed images. Formulas are given elsewhere.[11]

Average images are generated for both the 150 initial images and the 150 delayed images. The appropriate average is subtracted from each of the initial and delayed images, so that the correlations are of the fluctuations from the local mean. A two-dimensional region, denoted by (s_{ref}, n_{ref}), is defined in the initial fluctuation image. The signal at each pixel in this region is then correlated with the signals at various streamwise displacements $(s_{ref} + ds, n_{ref})$ in the delayed image. The correlation for each pixel in (s_{ref}, n_{ref}) is averaged with those of pixels falling on the same horizontal line in (s_{ref}, n_{ref}), so that the correlation at a point (ds, n_{ref}) reflects the cumulative correlation of a horizontal line at vertical position n_{ref} shifted a streamwise distance ds in the delayed image. This process is repeated for each horizontal line in (s_{ref}, n_{ref}). The resulting correlations are then averaged over the 150 image pairs and normalized by the maximum resulting coefficient for convenience. Thus, a correlation coefficient of 1.0 does not imply perfect correlation.

Correlation contours obtained in the flat plate boundary layer with a time delay of 25.0 μs are presented in Fig. 13a. For all of the double-pulse correlation fields, the streamwise direction is from left to right. In performing the correlations, δ_{vis} at the center of the ensemble images (11.8 mm in this case) was adopted as a length scale. The two-dimensional region was defined with a streamwise width of $\delta_{vis}/2$ as greater widths produced negligible differences in the correlation fields despite the added computation time. The point corresponding to maximum correlation in Fig. 13a occurs at $n/\delta_{vis} = 0.58$ and corresponds to a velocity of 610 m/s. For the given spatial magnification and time delay, a pixel element corresponds to a velocity difference of 9.4 m/s. This quantity is adopted as the uncertainty, resulting in 610 ± 10 m/s.

The presence of significant correlation levels at displacements corresponding to velocities greater than the freestream value is not surprising. If a convecting thin vertical line were correlated, the correlation would quickly peak at the optimal displacement and then quickly return to negligible levels. However, for structures of significant streamwise extent, the transition from negligible levels to the peak and back is more gradual. Another possible reason comes from the cited entrainment of freestream fluid at the front of the structures. The apparent increase in structure size caused by the condensation destruction may be interpreted in the correlation as an additional displacement. Further, the correlation is unconditional. If freestream fluid occupies the correlated region, the optimal displacement will correspond to the freestream velocity.

Spina and Smits[17] showed that large-scale structures maintain their identity for at least 1.5δ by analyzing streamwise-separated patterns of conditionally sampled mass-flux fluctuations and wall pressure fluctuations. For the 50.0 μs delay, a structure would convect 30 mm at 600 m/s. Despite traveling approximately 3δ_{vis}, almost all structures are easily tracked from initial to delayed image. The correlation field for a 50.0 μs delay ensemble is presented in

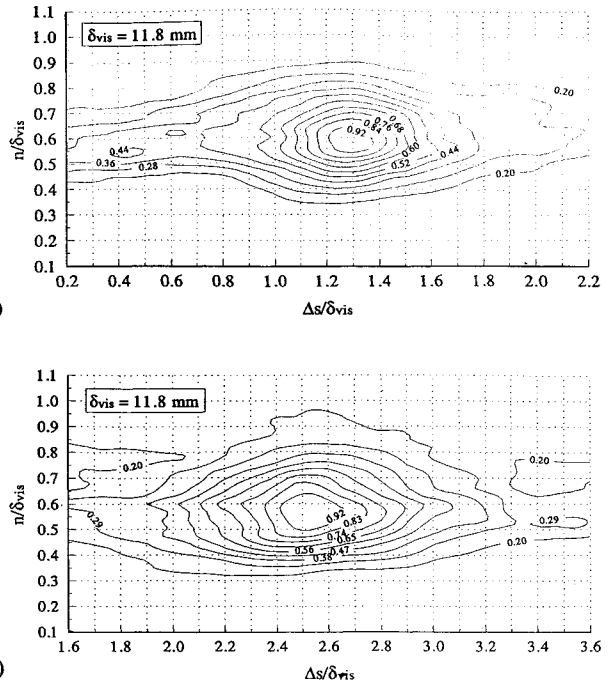

Fig. 13 Correlation fields calculated from ensembles of double-pulse images obtained in the flat plate boundary layer with a time delay of a) 25.0 μs and b) 50.0 μs.

Fig. 13b. The velocity obtained from the maximum correlation point, which occurs at $n/\delta_{vis} = 0.59$, is 595 ± 5 m/s.

To draw relevant comparisons, the delays employed downstream of the centered expansions were chosen so the structures would convect a similar distance. Accordingly, the 25.0 μs flat plate delay was scaled to 23.9 and 23.0 μs downstream of the 7-deg and 14-deg centered expansions, respectively, based on the ratio of freestream velocities across the expansions (obtained from a standard inviscid analysis). Downstream of the 7-deg centered expansion, the correlation fields are similar to those for the flat plate boundary layer. Delays of 16.0, 23.9, and 47.9 μs gave convection velocities of 590 ± 13, 620 ± 9, and 615 ± 5 m/s with the maximum correlation points at $n/\delta_{vis} = 0.73$, 0.71, and 0.71, all given respectively ($\delta_{vis} = 14.0$ mm).

That the maximum correlation point occurs at $n/\delta_{vis} = 0.6$–0.7 in the flat plate and 7-deg centered expansion boundary layers suggests the large-scale structures were mainly responsible for the correlations. Further, the derived convection velocities are reasonable. The unconditional nature of the correlations and modest sample sizes must be kept in mind when considering the importance of the actual velocity values. The differences between these convection velocities and those derived by Dawson et al.[10] from correlations of wall pressure fluctuations in these flows are too large to be accounted for by these sources of uncertainty. Clearly, the fluctuations responsible for Dawson et al.'s[10] correlations cannot be directly linked to the large-scale features responsible for the double-pulse correlations.

The correlation field for an ensemble with a time delay of 23.0 μs downstream of the 14-deg centered expansion (CO_2 condensation present) gave a convection velocity of 500 ± 10 m/s at $n/\delta_{vis} = 0.94$ ($\delta_{vis} = 22.3$ mm). The lack of identifiable large-scale features (Fig. 6c) resulted in the confinement of significant correlation levels to a thin region near the CO_2 condensation/no-condensation interface. The apparent deceleration across the 14-deg centered expansion runs counter to the acceleration detected by correlations of wall pressure fluctuations.[10] Again it appears the CO_2 condensation represents the boundary layer quite differently than the H_2O condensation. It is possible the CO_2 condensation occurs below the top edge of the velocity boundary layer, which could result in convection velocities much lower than the freestream velocity. Support for this idea comes from the fact that the boundary-layer thicknesses defined from the average intensity profiles (Fig. 9) are very comparable downstream of the 7-deg and 14-deg centered expansions despite the fact that schlieren images show the 14-deg centered expansion boundary layer is much thicker. Mean velocity and turbulence LDV measurements to be acquired in these flow fields should allow further insight.

Conclusions

The effects of four expansion regions [centered and gradual ($R/\delta_0 \simeq 50$) 7-deg and 14-deg expansions] on a Mach 3 fully developed, compressible turbulent boundary layer were studied. Visualizations were acquired utilizing H_2O condensation present in the freestream and absent in the higher temperature boundary layer. Mean and rms intensity profiles confirm the condensation signal is most closely related to temperature. The occurrence of CO_2 condensation downstream of the 14-deg expansions made the visualizations difficult to interpret.

The elongated longitudinal structures shown previously to populate the flat plate boundary layer[18] were also present downstream of the expansion regions, both with and without the flow conditioning assembly installed, and were not noticeably different from those of the flat plate boundary layer. Small-scale motions in the incoming boundary layer appear to be quenched very quickly by the expansion regions. Large-scale structures experience an increase in scale across the expansion regions commensurate with the increase in boundary-layer thickness. This is indicated by a similar dimensionless extent of spatial correlations in the flat plate and 7-deg centered expanded boundary layers when normalized with local length scales. No strong differences between the centered and gradual expansions of the same total deflection were evident in the visualizations. Spatial correlations in the flat plate boundary layer suggest the large-scale structure angle is approximately 45 deg. Visualizations suggest the angle increases across the expansion, but spatial correlations downstream of the 7-deg centered expansion show this increase may be short lived. Convection velocities from double-pulse correlations are reasonable for the flat plate and 7-deg centered expansion boundary layers.

Acknowledgment

This work is supported by the Air Force Office of Scientific Research (Contracts AFOSR-91-0412 and F49620-94-1-0074) with L. Sakell as contract monitor.

References

[1]Spina, E. F., Smits, A. J., and Robinson, S. K., "The Physics of Supersonic Turbulent Boundary Layers," *Annual Review of Fluid Mechanics*, Vol. 26, 1994, pp. 287–319.

[2]Bradshaw, P., "The Effect of Mean Compression or Dilatation on the Turbulence Structure of Supersonic Boundary Layers," *Journal of Fluid Mechanics*, Vol. 63, Pt. 3, 1974, pp. 449–464.

[3]Smits, A. J., and Wood, D. H., "The Response of Turbulent Boundary Layers to Sudden Perturbations," *Annual Review of Fluid Mechanics*, Vol. 17, 1985, pp. 321–358.

[4]Morkovin, M. V., "Effects of High Acceleration on a Turbulent Supersonic Shear Layer," Heat Transfer and Fluid Mechanics Inst., Stanford Univ., Stanford, CA, 1955.

[5]Thomann, H., "Effect of Streamwise Wall Curvature on Heat Transfer in a Turbulent Boundary Layer," *Journal of Fluid Mechanics*, Vol. 33, Pt. 2, 1968, pp. 283–292.

[6]Dussauge, J. P., and Gaviglio, J., "The Rapid Expansion of a Supersonic Turbulent Flow: Role of Bulk Dilatation," *Journal of Fluid Mechanics*, Vol. 174, 1987, pp. 81–112.

[7]Smith, D. R., and Smits, A. J., "The Rapid Expansion of a Turbulent Boundary Layer in a Supersonic Flow," *Theoretical Computational Fluid Dynamics*, Vol. 2, 1991, pp. 319–328.

[8]Johnson, A. W., "Laminarization and Retransition of Turbulent Boundary Layers in Supersonic Flow," Ph.D. Dissertation, Yale Univ., New Haven, CT, 1993.

[9]Arnette, S. A., Samimy, M., and Elliott, G. S., "The Effect of Expansion on the Large Scale Structure of a Compressible Turbulent Boundary Layer," AIAA Paper 93-2991, July 1993.

[10]Dawson, J. D., Samimy, M., and Arnette, S. A., "The Effects of Expansion on a Supersonic Boundary Layer: Surface Pressure Measurements," *AIAA Journal*, Vol. 32, No. 11, 1994, pp. 2169–2177.

[11]Arnette, S. A., Samimy, M., and Elliott, G. S., "Expansion Effects on Supersonic Boundary Layers," Ohio State Univ., Internal Report MEMS-94-101, Columbus, OH, Feb. 1994.

[12]Narasimha, R., and Viswanath, P. R., "Reverse Transition at an Expansion Corner in Supersonic Flow," *AIAA Journal*, Vol. 13, No. 5, 1975, pp. 693–695.

[13]Narasimha, R., and Sreenivasan, K. R., "Relaminarization in Highly Accelerated Turbulent Boundary Layers," *Journal of Fluid Mechanics*, Vol. 61, Pt. 3, 1973, pp. 417–447.

[14]Spina, E. F., Donovan, J. F., and Smits, A. J., "On the Structure of High-Reynolds-Number Supersonic Turbulent Boundary Layers," *Journal of Fluid Mechanics*, Vol. 222, 1991, pp. 293–327.

[15]Lee, S., Lele, S. K., and Moin, P., "Simulation of Spatially Evolving Turbulence and the Applicability of Taylor's Hypothesis in Compressible Flow," *Physics of Fluids A*, Vol. 4, No. 7, 1992, pp. 1521–1530.

[16]Robinson, S. K., "Coherent Motions in the Turbulent Boundary Layer," *Annual Review of Fluid Mechanics*, Vol. 23, 1991, pp. 601–639.

[17]Spina, E. F., and Smits, A. J., "Organized Structures in a Compressible, Turbulent Boundary Layer," *Journal of Fluid Mechanics*, Vol. 182, 1987, pp. 85–109.

[18]Samimy, M., Arnette, S. A., and Elliott, G. S., "Streamwise Structures in a Turbulent Supersonic Boundary Layer," *Physics of Fluids*, Vol. 6, No. 3, 1994, pp. 1081–1083.

[19]Samimy, M., Elliott, G. S., Glawe, D. D., Reeder, M. F., and Arnette, S. A., "Compressible Mixing Layers With and Without Particles," Ohio State Univ. Internal Report MEMS-92-101 Columbus, OH, Aug. 1992.

[20]Smith, M., Smits, A., and Miles, R., "Compressible Boundary-Layer Density Cross Sections by UV Rayleigh Scattering," *Optics Letters*, Vol. 14, No. 17, 1989, pp. 916–918.

[21]Miles, R. B., Lempert, W. R., and Forkey, J., "Instantaneous Velocity Fields and Background Suppression by Filtered Rayleigh Scattering," AIAA Paper 91-0357, Jan. 1991.

[22]Arnette, S. A., Samimy, M., and Elliott, G. S., "On Streamwise Vortices in High Reynolds Number Supersonic Axisymmetric Jets," *Physics of Fluids A*, Vol. 5, No. 1, 1993, pp. 187–202.

[23]Elliott, G. S., Samimy, M., and Arnette, S. A., "Study of Compressible Mixing Layers Using Filtered Rayleigh Scattering Based Visualizations," *AIAA Journal*, Vol. 30, No. 10, 1992, pp. 2567–2569.

[24]Miles, R. B., Forkey, J., and Lempert, W. R., "Filtered Rayleigh Scattering Measurements in Supersonic/Hypersonic Facilities," AIAA Paper 92-3894, July 1992.

[25]Elliott, G. S., Samimy, M., and Arnette, S. A., "Filtered Rayleigh Scattering Based Measurements in Compressible Mixing Layers," AIAA Paper 92-3543, July 1992.

[26]Elliott, G. S., Samimy, M., and Arnette, S. A., "Molecular Filter-Based Diagnostics in High Speed Flows," AIAA Paper 93-0512, Jan. 1993.

[27]Cogne, S., Forkey, J., Lempert, W., Miles, R. B., and Smits, A. J., "The Evolution of Large-Scale Structures in a Supersonic Turbulent Boundary Layer," *Proceedings of the Symposium on Transitional and Turbulent Compressible Flows*, American Society of Mechanical Engineers, Fluids Engineering Conference, 1993.

[28]Forkey, J., Cogne, S., Smits, A., Bogdonoff, S., Lempert, W. R., and Miles, R. B., "Time-Sequenced and Spectrally Filtered Rayleigh Imaging of Shock Wave and Boundary Layer Structure for Inlet Characterization," AIAA Paper 93-2300, June 1993.

[29]Elliott, G. S., Samimy, M., and Arnette, S. A., "The Evolution of Large Scale Structures in Compressible Mixing Layers," Ninth Turbulent Shear Flow Conference, Kyoto, Japan, Aug. 1993, Paper 19-4.

[30]Falco, R. E., "Coherent Motions in the Outer Region of Turbulent Boundary Layers," *Physics of Fluids*, Vol. 20, No. 10, Pt. 2, 1977, pp. S124–S132.

[31]Smith, M. W., and Smits, A. J., "Cinematic Visualization of Coherent Density Structures in a Supersonic Turbulent Boundary Layer," AIAA Paper 88-0500, Jan. 1988.

[32]Robinson, S. K., "Space-Time Correlation Measurements in a Compressible Turbulent Boundary Layer," AIAA Paper 86-1130, 1986.

[33]Wegener, P. P., and Mack, L. M., "Condensation in Supersonic and Hypersonic Wind Tunnels," *Advances in Applied Mechanics*, edited by H. L. Dryden and T. von Kármán, Academic, New York, Vol. 5, 1958, pp. 307–447.

[34]Laderman, A. J., and Demetriades, A., "Turbulent Shear Stresses in Compressible Boundary Layers," *AIAA Journal*, Vol. 17, No. 7, 1979, pp. 736–744.

[35]Kistler, A. L., "Fluctuation Measurements in a Supersonic Turbulent Boundary Layer," *Physics of Fluids*, Vol. 2, No. 3, 1959, pp. 290–296.